Modal Source Radiator Model for Arbitrary Two-Dimensional Arrays of Subwavelength Apertures on Metal Films

Takuo Tanemura, *Member, IEEE*, Pierre Wahl, Shanhui Fan, *Fellow, IEEE*, and David A. B. Miller, *Fellow, IEEE*

(Invited Paper)

***Abstract*—We present a theoretical and numerical framework to analyze optical properties of subwavelength apertures that are distributed arbitrarily on the 2-D plane of a metal film. Using the radiation patterns linked to individual eigenmodes inside the aperture, the coupling between multiple apertures is described efficiently by a small-rank linear system of equations. The complicated contributions from both the surface plasmon polariton (SPP) and creeping wave are inherently included in the analysis. Three-dimensional fully vectorial finite-difference time-domain calculations are used to verify the model in several test cases. The model accurately predicts all the salient features in extraordinary optical transmission (EOT) spectra of 2-D nanoslit arrays, including the surface plasmon resonances and Rayleigh–Wood anomalies. We also explore the effects of finite array size on EOT and discover a novel regime where the EOT efficiency decreases with an increasing number of apertures. Finally, we apply the model in calculating SPP excitation by an arbitrarily patterned nanoslit array. The presented method not only provides deeper physical insights into EOT and related phenomena, but should also be useful in designing a variety of novel aperiodic plasmonic devices with drastically less computational cost.**

***Index Terms*—Electromagnetic theory, optical scattering, optical surface waves, plasmons.**

I. Introduction

THE optical properties of metallic films perforated by subwavelength apertures have attracted great research interest in recent years. Due to the strongly confined cavity mode resonances inside the apertures and the surface plasmon polaritons (SPPs) that give complex coupling between multiple apertures, these nanometallic structures provide a variety of interesting physical phenomena, such as extraordinary optical transmission (EOT) [1], beaming [2], and negative refraction [3]. With the recent progress in nanofabrication technologies, there is a growing interest to exploit these effects at infrared and visible regimes with potential applications including subwavelength sensing [4]–[6], enhanced light emission [7], [8], ultracompact photodetection for optical interconnects [9]–[11], and light trapping in solar cells [12], [13].

While the initial studies on EOT have focused on infinitely large periodic arrays, it was subsequently found that finite-sized arrays with less or even no periodicity also exhibit similar EOT behaviors. Ruan and Qiu carried out a rigorous 3-D finite-difference time-domain (FDTD) simulation on randomly distributed holes to find out that the localized waveguide resonance inside each hole can mediate enhanced transmission even in the absence of periodicity [14]. The EOT phenomenon in aperiodic arrays has also been confirmed experimentally in the optical [15], [16] and terahertz [17] regimes. On the application side, various aperiodic structures have been investigated to provide unique device functionalities. Arrays of spatially varying subwavelength apertures on metallic films have been used for planar lenses [18], [19] and angle compensation [20]. In the recent work of our own, we have employed an aperiodic nanoslit array to demonstrate a wavelength-splitting plasmonic detector with a discrete spectral response, which is not readily possible with periodic approaches [21].

Despite these findings and unique potentials of aperiodic nanometallic structures, though a large part of this study has been devoted to studying periodic arrays, the aperiodic counterparts have been left relatively unexplored. This is largely due to the difficulty in analyzing large-area arrays without periodicity. In the pioneering work by Garcia-Vidal *et al.*, the modal expansion technique was used to study 2-D aperiodic arrays of holes in perfect conductor films [22]–[24]. The model was also extended to real metals by imposing the surface impedance boundary condition (SIBC) at the metal-dielectric interfaces [24]–[26]. While this method has been proved extremely powerful in capturing approximate behaviors, the SIBC approximation could often lead to relatively large quantitative errors (e.g., see [26], Fig. 1]). On the other hand, a microscopic model based on the scattering-matrix concept was developed by Liu and Lalanne to analyze SPP interactions on the real metal surfaces with

Manuscript received July 11, 2012; revised October 1, 2012; accepted November 12, 2012. Date of publication January 9, 2013; date of current version April 25, 2013. This work was supported in part by the Air Force Office of Scientific Research Robust and Complex On-Chip Nanophotonics MURI under Grant FA9550-09-1-0704 and the Interconnect Focus Center, one of six research centers funded under the Focus Center Research Program, a Semiconductor Research Corporation entity. The work of T. Tanemura was supported by the Japan Society for the Promotion of Science.

T. Tanemura is with the Department of Electrical Engineering and Information Systems, The University of Tokyo 113-8654, Japan (e-mail: tanemura@ee.t.u-tokyo.ac.jp).

P. Wahl is with the Brussels Photonics Team, Department of Applied Physics and Photonics, TONA-FIRW, Vrije Universiteit Brussel, 1030 Brussels, Belgium (e-mail: pwahl@b-phot.org).

S. Fan and D. A. B. Miller are with the Edward L. Ginzton Laboratory, Stanford University, Stanford, CA 94305 USA (e-mail: shanhui@stanford.edu; dabm@stanford.edu).

Color versions of one or more of the figures in this paper are available online at http://ieeexplore.ieee.org.

Digital Object Identifier 10.1109/JSTQE.2012.2229383

higher precision [27], [28]. A similar model has also been used to study light scattering from aperiodically located multiple grooves [29]. Since these models assume SPP waves (or SPP Bloch waves) propagating along a fixed direction, however, their applicability is limited to 1-D arrays [29] or an array of 1-D periodic chains [28].

As a result, for quantitative analyses of fully aperiodic 2-D arrays in real metal films, one must usually rely on rigorous fully vectorial 3-D numerical simulations, e.g., FDTD [14], [25], [26], [30], finite difference frequency domain [29], rigorous coupled wave analysis (RCWA) [27], [28], [31], and Green's tensor approaches [32]–[37]. While FDTD method has been particularly popular due to its straightforward and versatile implementation, such a brute-force simulation rarely provides an intuitive picture of underlying physics. Moreover, the computation becomes extremely demanding for large-area aperiodic arrays, and limits the range of structures that we could explore. Unlike the other approaches, the Green's tensor methods require discretization only at the scattering elements, and are particularly suited in analyzing thin metal films [32]–[37]. Nevertheless, they still involve solution of a relatively large system of equations, which could typically be computationally expensive, especially as the number of scatterers increases [35], [36]. In addition, solving the Green's tensor in a metallic stratified structure is generally a nontrivial problem and requires a special care to achieve numerical convergence [37]–[39]. It is, therefore, of great value to develop a simple and rapid numerical method with sufficient precision that could be scaled to explore large-area aperiodic nanometallic structures.

In this paper, we present a novel efficient and straightforward method of computing the transmission and scattering properties through multiple subwavelength apertures that are arbitrarily distributed on an optically thick metal film. Our method consists of two steps. First, we treat each aperture as a modal source radiator, which has its own characteristic radiation patterns linked to individual eigenmodes of the aperture. Then, by imposing the boundary conditions at the metal-dielectric interfaces, we derive a linear system of equations to solve for a self-consistent solution. While we base our model on the conventional Green's function scattering theory, we are not interested in deriving the Green's function itself. Instead, we numerically extract the radiation patterns from individual eigenmodes of a single isolated aperture and employ these radiation patterns to calculate the coupling between multiple apertures at arbitrary locations. As a result, our model automatically includes the complicated contributions from both the SPP wave and the residual so-called creeping wave (also called Norton wave or quasi-cylindrical wave) [40]–[48]. Since these two types of waves propagate at a metal surface obeying different power-decay laws, they contribute differently depending on the wavelength and the distance between the apertures: generally, the coupling is mediated by the SPP at intermediate distances, whereas the creeping wave dominates at distances shorter than a wavelength or longer than the propagation length of SPP (typically a few tens of wavelengths). The coexistence of these two waves, as well as their complex cross-conversion processes at the apertures [44] has often been the major obstacle against simple analytic modeling of multiple-aperture interactions.

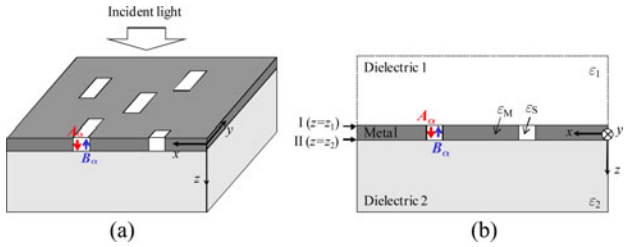

Fig. 1. (a) Schematic picture and (b) the cross-sectional view of the structures studied in this paper.

In light of the underlying concept, the model presented in this paper is similar to the Green's tensor method [32] (which is also closely related to the coupled dipole approximation or the discrete dipole approximation [49], [50]). They are both based on the Green's function formulation and approximate the entire set of scattering elements by a finite number of dipoles or radiators to derive linear systems of equations. The strategy of discretization, however, is very different. In the Green's tensor method, the scattering elements are discretized into small polarizable dipoles, resulting in typically a very large matrix equation system. The present method, in contrast, uses the eigenmodes of each aperture as the basis functions in the discretization, and analyzes the coupling between these finite-sized radiators instead of point dipoles. Owing to the limited number of relevant eigenmodes inside the subwavelength apertures, we gain a significant reduction in the size of the matrix.

This paper is organized as follows: In Section II, we present our formalism by starting with the general Green's function theory (see Section II-A) and explain the numerical method of deriving all the necessary parameters (see Section II-B). In Section III, we test the method in calculating the optical properties of finite-sized aperiodic arrays of rectangular slits and compare the results with the exact solutions obtained by fully vectorial 3-D FDTD. We show that our method is quantitatively accurate over a broad spectral range (400–1200 nm) below the plasma frequency of the metal.

II. Theoretical Framework

A. Formulation of Modal Source Radiator Model

The structure analyzed in this paper is shown schematically in Fig. 1. Although our theory should be applicable to apertures with different geometries, we assume an array of identical subwavelength rectangular slits here for simplicity and for ease of explanation.

We start by expressing the relative dielectric tensor of the entire system as

$$\varepsilon(\mathbf{r},\omega) \equiv \varepsilon_{\mathrm{B}}(\mathbf{r},\omega) + \Delta\varepsilon(\mathbf{r},\omega). \tag{1}$$

Here, $\varepsilon_{\mathrm{B}}(\mathbf{r},\omega)$ and $\Delta\varepsilon(\mathbf{r},\omega)$ denote the frequency-dependent dielectric tensor of the background and scattering systems at position $\mathbf{r}$. For the case depicted in Fig. 1, $\varepsilon_{\mathrm{B}}(\mathbf{r},\omega)$ describes the background layered structure (i.e., an unpatterned metal layer and top and bottom dielectric layers) without the slits and $\Delta\varepsilon(\mathbf{r},\omega)$ denotes the perturbation to this system associated with adding slits; $\Delta\varepsilon = \varepsilon_{\mathrm{S}} - \varepsilon_{\mathrm{M}}$ inside the aperture and 0

elsewhere, where $\varepsilon_{\rm M}$ and $\varepsilon_{\rm S}$ are the relative dielectric tensors of the metal and the material inside the slits, respectively. Under a monochromatic field excitation with exp(–*i*ωt) time dependence, the complex amplitude of electric field $\mathbf{E}(\mathbf{r},\omega)$ satisfies the vectorial wave equation:

$$\left[(\nabla\times\nabla\times)-k_0^2\varepsilon(\mathbf{r},\omega)\right]\mathbf{E}(\mathbf{r},\omega)=i\omega\mathbf{J}(\mathbf{r},\omega) \tag{2}$$

where k_0 is the wave number in vacuum and $\mathbf{J}$ represents the current source, which is responsible for the excitation field. Inserting (1) into (2), and using the usual Green's function formalism, we obtain the Lippmann–Schwinger equation [32], [34]

$$\mathbf{E}(\mathbf{r})=\mathbf{E}_0(\mathbf{r})+k_0^2\int d\mathbf{r}'\mathbf{G}(\mathbf{r},\mathbf{r}')\Delta\varepsilon(\mathbf{r}')\mathbf{E}(\mathbf{r}') \tag{3}$$

where we have dropped the explicit dependence on the frequency ω for simplicity of notation. $\mathbf{E}_0(\mathbf{r})$ is the electric field in the absence of apertures, so that

$$\left[(\nabla\times\nabla\times)-k_0^2\varepsilon_{\rm B}(\mathbf{r})\right]\mathbf{E}_0(\mathbf{r})=i\omega\mathbf{J}(\mathbf{r}). \tag{4}$$

Unlike the usual definition of Green's dyad in a homogeneous medium, $\mathbf{G}(\mathbf{r},\mathbf{r}')$ in (3) is the Green's dyad associated with the background system $\varepsilon_{\rm B}(\mathbf{r})$, and is defined by

$$\left[(\nabla\times\nabla\times)-k_0^2\varepsilon_{\rm B}(\mathbf{r})\right]\mathbf{G}(\mathbf{r},\mathbf{r}')=\delta(\mathbf{r}-\mathbf{r}') \tag{5}$$

where $\delta(\mathbf{r}-\mathbf{r}')$ describes a point vector source at position $\mathbf{r}'$. Note that the integral on the right-hand side of (3) is restricted to the volume inside the slits, since $\Delta\varepsilon$ vanishes outside the slits. From (3) and the Maxwell's equation $\mathbf{H}=(1/i\omega\mu)\nabla\times\mathbf{E}$, we can similarly express the magnetic field as

$$\mathbf{H}(\mathbf{r})=\mathbf{H}_0(\mathbf{r})+\int d\mathbf{r}'\mathbf{G}_{\rm H}(\mathbf{r},\mathbf{r}')\mathbf{E}(\mathbf{r}') \tag{6}$$

where the linear operator $\mathbf{G}_{\rm H}(\mathbf{r},\mathbf{r}')$ relates the radiated magnetic field at arbitrary $\mathbf{r}$ to the electric field at $\mathbf{r}'$ (inside the slit). Note also that the term $k_0^2\Delta\varepsilon$ in (3) has been absorbed in the definition of $\mathbf{G}_{\rm H}(\mathbf{r},\mathbf{r}')$ in (6) for simplicity of notation. Using a Dirac notation, (6) is conveniently written as

$$|\mathbf{H}\rangle=|\mathbf{H}_0\rangle+\mathbf{G}_{\rm H}|\mathbf{E}\rangle. \tag{7}$$

Now, let us express the fields in the metal layer $(z_1\le z\le z_2)$ as a superposition of the eigenmodes of the slits, i.e., the guided modes that would propagate vertically in $\pm z$ directions inside the slit. Inside the slits, we have the expansions

$$\begin{aligned}|\mathbf{E}\rangle&=\sum_\alpha\left(A_\alpha e^{iq_\alpha z}|\mathbf{e}_\alpha^+\rangle+B_\alpha e^{-iq_\alpha z}|\mathbf{e}_\alpha^-\rangle\right)\\ |\mathbf{H}\rangle&=\sum_\alpha\left(A_\alpha e^{iq_\alpha z}|\mathbf{h}_\alpha^+\rangle+B_\alpha e^{-iq_\alpha z}|\mathbf{h}_\alpha^-\rangle\right).\end{aligned} \tag{8}$$

Here, the index α runs over all the slits and eigenmodes and q_α is the propagation constant of a given eigenmode, which is generally complex. A_α and B_α are the complex amplitude of the forward and backward propagating mode and $\mathbf{e}_\alpha^\pm$ ($\mathbf{h}_\alpha^\pm$) are the electric (magnetic) field profiles of these modes, which are therefore vector functions of the transverse (*xy* plane) position in the slit. In writing (8), we are implicitly assuming that the adjacent slits are separated by a sufficient distance (more than several times the skin depth), so that the direct coupling through the metal between the waves propagating inside the slits is negligible.

From the symmetry properties of the forward- and backward-propagating modes in a reciprocal system, we can decompose $\mathbf{e}_\alpha^\pm$ and $\mathbf{h}_\alpha^\pm$ into transverse (*xy* plane) and longitudinal (z) components, which we denote here by subscripts t and z, such that $\mathbf{e}_\alpha^\pm=\mathbf{e}_{{\rm t}\alpha}\pm e_{z\alpha}\hat{\mathbf{z}}$ and $\mathbf{h}_\alpha^\pm=\pm\mathbf{h}_{{\rm t}\alpha}+h_{z\alpha}\hat{\mathbf{z}}$ [51, p. 212]. Using these relations, the transverse components in (8) are written as

$$\begin{aligned}|\mathbf{E}_{\rm t}\rangle&=\sum_\alpha\left(A_\alpha e^{iq_\alpha z}+B_\alpha e^{-iq_\alpha z}\right)|\mathbf{e}_{{\rm t}\alpha}\rangle,\\ |\mathbf{H}_{\rm t}\rangle&=\sum_\alpha\left(A_\alpha e^{iq_\alpha z}-B_\alpha e^{-iq_\alpha z}\right)|\mathbf{h}_{{\rm t}\alpha}\rangle.\end{aligned} \tag{9}$$

Due to the Lorentz reciprocity of the system, we have the modal orthogonality relation [51, p. 605]

$$\langle\mathbf{e}_{{\rm t}\alpha}\,|\mathbf{h}_{{\rm t}\beta}\rangle\equiv\int(\mathbf{e}_{{\rm t}\alpha}\times\mathbf{h}_{{\rm t}\beta})\cdot\hat{\mathbf{z}}dxdy=\delta_{\alpha\beta} \tag{10}$$

where $\delta_{\alpha\beta}$ is the Kronecker delta function and we assume that $\mathbf{e}_{{\rm t}\alpha}$ and $\mathbf{h}_{{\rm t}\alpha}$ are properly normalized. Note that we have employed the unconjugated form for the definition of the inner product $\langle\mathbf{e}_{{\rm t}\alpha}|\,\mathbf{h}_{{\rm t}\alpha}\rangle$, so that (10) is valid for a lossy metallic waveguide as well [51, p. 605]. Also, we have once again used the assumption that the adjacent slits are separated by a sufficient distance, so that the inner product of two modes in different slits can be approximated to be zero. As a result, $\{|\mathbf{e}_{{\rm t}\alpha}\rangle,|\mathbf{h}_{{\rm t}\alpha}\rangle\}$ in (9) constitutes (at least approximately) an orthogonal set. On the other hand, it is by no means complete in a sense that the superposition of $\{|\mathbf{e}_{{\rm t}\alpha}\rangle,|\mathbf{h}_{{\rm t}\alpha}\rangle\}$ cannot describe arbitrary fields inside the metal. (We must also include the continuous spectrum to constitute a complete set [52].) We should stress, however, that only the fields inside the slits are necessary here, because, as we have discussed, $\Delta\varepsilon$ in (3) vanishes outside the slits. The fields inside the slits should be expressed by (9) with sufficient accuracy, provided we include all the necessary waveguide modes. This feature is a significant advantage of our method compared with other mode-expansion techniques (such as RCWA), which generally require much larger number of modes to describe the field accurately even inside the metal.

We are now interested in the transverse magnetic field at the two boundaries, I ($z=z_1$) and II ($z=z_2$) as defined in Fig. 1. By inserting (8) into (7), and letting $z=z_1$, we obtain an expression for the magnetic field at the interface I:

$$\left|\mathbf{H}_{\rm t}^{\rm I}\right\rangle=\left|\mathbf{H}_0^{\rm I}\right\rangle+\sum_\alpha\left(A_\alpha e^{iq_\alpha z_1}\mathbf{G}^{\rm I}\left|\mathbf{e}_\alpha^+\right\rangle+B_\alpha e^{-iq_\alpha z_1}\mathbf{G}^{\rm I}\left|\mathbf{e}_\alpha^-\right\rangle\right). \tag{11}$$

$\left|\mathbf{H}_{\rm t}^{\rm I}\right\rangle$ is the transverse magnetic field at the interface I for the background structure and $\mathbf{G}^{\rm I}\left|\mathbf{e}_\alpha^\pm\right\rangle$ is defined in the position basis as

$$\left\langle\mathbf{r}^{\rm I}\right|\mathbf{G}^{\rm I}\left|\mathbf{e}_\alpha^\pm\right\rangle\equiv\int d\mathbf{r}'\mathbf{G}_{\rm tH}(\mathbf{r}^{\rm I},\mathbf{r}')e^{\pm iq(z'-z_1)}\mathbf{e}_\alpha^\pm(x',y') \tag{12}$$

where $\mathbf{r}^{\rm I}$ is an arbitrary position in the *xy* plane at the interface I ($z=z_1$) and $\mathbf{G}_{\rm tH}$ describes only the transverse (x and y) magnetic components of $\mathbf{G}_{\rm H}$ defined in (6). Similarly, expressions for the interface II are derived by replacing z_1 with z_2 and the superscript I with II in (11).

Finally, we impose the boundary conditions that $\mathbf{H}_{\mathrm{t}}$ should be continuous at the two interfaces I and II above and below the slits. By equating (9) with (11) at $z = z_1$, applying $\langle \mathbf{e}_{t\alpha} |$ on both sides, and using (10), we obtain a linear system of equations for the unknowns $\{A_\alpha, B_\alpha\}$. We can write these equations more conveniently by using a new set of variables $\{C_\alpha, D_\alpha\}$ defined by

$$C_\alpha \equiv A_\alpha e^{iq_\alpha z_1} - B_\alpha e^{-iq_\alpha z_1}, D_\alpha \equiv A_\alpha e^{iq_\alpha z_2} - B_\alpha e^{-iq_\alpha z_2}. \tag{13}$$

The linear system of equations for the unknowns $\{C_\alpha, D_\alpha\}$ is then written as

$$\begin{pmatrix} C_\alpha \\ D_\alpha \end{pmatrix} = \begin{pmatrix} \langle \mathbf{e}_{\mathrm{t}\alpha} \mid \mathbf{H}_0^{\mathrm{I}} \rangle \\ \langle \mathbf{e}_{\mathrm{t}\alpha} \mid \mathbf{H}_0^{\mathrm{II}} \rangle \end{pmatrix} + \sum_\beta \begin{pmatrix} \kappa_{\alpha\beta}^{11} & \kappa_{\alpha\beta}^{12} \\ \kappa_{\alpha\beta}^{21} & \kappa_{\alpha\beta}^{22} \end{pmatrix} \begin{pmatrix} C_\beta \\ D_\beta \end{pmatrix} \tag{14}$$

where β runs over all the slits and eigenmodes. From (9) and (13), C_α and D_α physically represent the magnetic field of respective modes at the two interfaces. The first term on the right-hand side of (14), thus, represents the modal excitation by the incident field, whereas the second term describes either the reflection of each eigenmode inside the aperture at the interfaces (when $\alpha = \beta$) or the coupling between different modes (when $\alpha \neq \beta$). The coupling coefficients $\kappa_{\alpha\beta}^{ij}$ are expressed explicitly as

$$\begin{aligned}
\kappa_{\alpha\beta}^{11} &= \frac{1}{a_{\beta+} - a_{\beta-}} \left(-a_{\beta-} \langle \mathbf{e}_{\mathrm{t}\alpha} | \mathbf{G}^{\mathrm{I}} | \mathbf{e}_\beta^+ \rangle - a_{\beta+} \langle \mathbf{e}_{\mathrm{t}\alpha} | \mathbf{G}^{\mathrm{I}} | \mathbf{e}_\beta^- \rangle \right) \\
\kappa_{\alpha\beta}^{12} &= \frac{1}{a_{\beta+} - a_{\beta-}} \left(\langle \mathbf{e}_{\mathrm{t}\alpha} | \mathbf{G}^{\mathrm{I}} | \mathbf{e}_\beta^+ \rangle + \langle \mathbf{e}_{\mathrm{t}\alpha} | \mathbf{G}^{\mathrm{I}} | \mathbf{e}_\beta^- \rangle \right) \\
\kappa_{\alpha\beta}^{21} &= \frac{1}{a_{\beta+} - a_{\beta-}} \left(-\langle \mathbf{e}_{\mathrm{t}\alpha} | \mathbf{G}^{\mathrm{II}} | \mathbf{e}_\beta^+ \rangle - \langle \mathbf{e}_{\mathrm{t}\alpha} | \mathbf{G}^{\mathrm{II}} | \mathbf{e}_\beta^- \rangle \right) \\
\kappa_{\alpha\beta}^{22} &= \frac{1}{a_{\beta+} - a_{\beta-}} \left(a_{\beta+} \langle \mathbf{e}_{\mathrm{t}\alpha} | \mathbf{G}^{\mathrm{II}} | \mathbf{e}_\beta^+ \rangle + a_{\beta-} \langle \mathbf{e}_{\mathrm{t}\alpha} | \mathbf{G}^{\mathrm{II}} | \mathbf{e}_\beta^- \rangle \right)
\end{aligned} \tag{15}$$

where we have defined $a_{\beta\pm} \equiv \exp\left[\pm i q_\beta (z_2 - z_1)\right]$ for convenience.

Our interest here is to analyze the optical properties of a finite set of apertures, which are arbitrarily located on the 2-D plane. Given an aperture with particular geometry, we first derive $q_\alpha, |\mathbf{e}_{\mathrm{t}\alpha}\rangle, \mathbf{G}^{\mathrm{I/II}} |\mathbf{e}_\alpha^\pm\rangle$ and store them in our database. At the same time, the background field $\left|\mathbf{H}_0^{\mathrm{I/II}}\right\rangle$ is obtained for the given excitation condition. Then, for arbitrary locations of the slits, we can explicitly calculate $\kappa_{\alpha\beta}^{ij}$ using (15) and solve (14). Once $\{C_\alpha, D_\alpha\}$ are obtained, the electromagnetic field at an arbitrary position can be calculated by using (3) and (6).

B. Numerical Method for Deriving the Parameters

Among all the necessary datasets, q_α and $|\mathbf{e}_{\mathrm{t}\alpha}\rangle$ can be obtained readily by solving the waveguide eigenmode of the aperture using any numerical 2-D mode solver and $|\mathbf{H}_0^{\mathrm{I/II}}\rangle$ is derived either analytically or by a single numerical simulation of the background structure. The only nontrivial terms are $\mathbf{G}^{\mathrm{I/II}} |\mathbf{e}_\alpha^\pm\rangle$, which, by definition (12), contain the Green's dyad of the background structure. The Green's dyad for a multiple-layered system, in general, cannot be expressed in a closed analytical form, and must be derived numerically by computing Sommerfeld integrals in the $\mathbf{k}$-space [38]. However, due to a number of singularities such as poles and branch cuts in these integrals, special attention and often iterative calculations are required to achieve numerical convergence [37]–[39]. In this paper, we instead propose an efficient and straightforward method of extracting $\mathbf{G}^{\mathrm{I/II}} |\mathbf{e}_\alpha^\pm\rangle$ directly through full-field numerical simulation of a single isolated aperture under several different conditions. Our method exploits the fact that we are actually not interested in the Green's dyad itself, but its operated functions $\mathbf{G}^{\mathrm{I/II}} |\mathbf{e}_\alpha^\pm\rangle$, which physically represent the radiated magnetic field patterns at the interfaces I and II generated by the individual eigenmodes $|\mathbf{e}_\alpha^\pm\rangle$.

We assume two main simplifications. First, the aperture is assumed to have subwavelength dimension, so that the wave propagation inside the aperture can be approximated by the fundamental (i.e., least evanescent) eigenmode, or at most, a few eigenmodes with symmetrical constraints. Such an assumption is justified in most of the interesting cases studied in the context of EOT, where we prefer to employ strongly resonant deeply subwavelength apertures to enhance transmission. Under this approximation, we can predominantly excite the mode of interest numerically with proper boundary conditions. Second, we assume that the metal film is thicker than the skin depth (typically, a few tens of nanometer). Since the Green's dyad $\mathbf{G}_{\mathrm{H}}(\mathbf{r},\mathbf{r}')$ in (12) decays exponentially as $\mathbf{r}'$ runs deeper inside the metal [note that $\mathbf{G}_{\mathrm{H}}(\mathbf{r},\mathbf{r}')$ is the Green's dyad defined for the background layered structure ε_{B} without the slits] and we presume this decay length is much shorter than our metal thickness, we can in practice extend the integration limit of z' to infinitely deep into the metal. As a consequence, $\mathbf{G}^{\mathrm{I/II}} |\mathbf{e}_\alpha^\pm\rangle$ are approximately independent on the metal thickness and we can employ infinitely thick metal to derive these parameters. Such an assumption has also been used in [46].

Fig. 2 schematically shows a set of numerical simulations we perform to extract $\mathbf{G}^{\mathrm{I/II}} |\mathbf{e}_\alpha^\pm\rangle$. First, we simulate the case of a single aperture on an infinitely thick metal with a light illuminating from the top [see Fig. 2(a)]. Due to the absence of any back-propagating wave, $B_\alpha = 0$. On the other hand, A_α can be extracted by applying $\langle \mathbf{e}_{\mathrm{t}\alpha} |$ to the magnetic field inside the slit. Since we have assumed that the fundamental mode (which we denote here by A_1) is excited predominantly, contributions from all other modes in the summation of (11) can be neglected. As a consequence, (11) in this case is written as

$$\left|\mathbf{H}_{\mathrm{t}}^{\mathrm{I}}\right\rangle = \left|\mathbf{H}_0^{\mathrm{I}}\right\rangle + A_1 e^{iq_1 z_1} \mathbf{G}^{\mathrm{I}} \left|\mathbf{e}_1^+\right\rangle \tag{16}$$

Since we know $A_1, q_1, |\mathbf{H}_{\mathrm{t}}^{\mathrm{I}}\rangle$, and $|\mathbf{H}_0^{\mathrm{I}}\rangle$, we can derive $\mathbf{G}^{\mathrm{I}}|\mathbf{e}_1^+\rangle$ using (16). In a similar manner, we extract $\mathbf{G}^{\mathrm{II}}|\mathbf{e}_1^-\rangle$ by extending the thickness in the upward direction and illuminating the structure from the bottom [see Fig. 2(b)]. Finally, we simulate the finite thickness case [see Fig. 2(c)] to derive $\mathbf{G}^{\mathrm{I}}|\mathbf{e}_1^-\rangle$ and $\mathbf{G}^{\mathrm{II}}|\mathbf{e}_1^+\rangle$. In this case, (11) is written as

$$\left|\mathbf{H}_{\mathrm{t}}^{\mathrm{I}}\right\rangle = \left|\mathbf{H}_0^{\mathrm{I}}\right\rangle + A_1 e^{iq_1 z_1} \mathbf{G}^{\mathrm{I}} \left|\mathbf{e}_1^+\right\rangle + B_1 e^{-iq_1 z_1} \mathbf{G}^{\mathrm{I}} \left|\mathbf{e}_1^-\right\rangle. \tag{17}$$

By inserting $A_1, B_1, q_1, |\mathbf{H}_{\mathrm{t}}^{\mathrm{I}}\rangle, |\mathbf{H}_0^{\mathrm{I}}\rangle$, and $\mathbf{G}^{\mathrm{I}}|\mathbf{e}_1^+\rangle$, we can derive $\mathbf{G}^{\mathrm{I}}|\mathbf{e}_1^-\rangle$. Similarly, $\mathbf{G}^{\mathrm{II}}|\mathbf{e}_1^+\rangle$ is obtained from the field at the

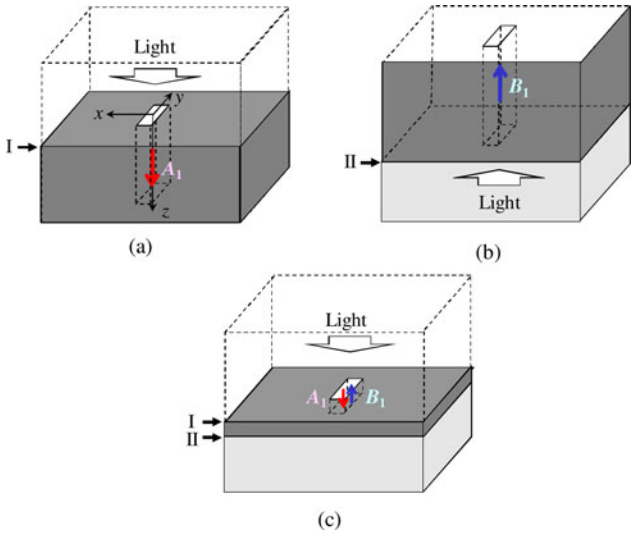

Fig. 2. Schematic pictures describing the series of numerical simulations to extract all four radiation patterns: (a) single slit in a downwardly infinitely thick metal to extract $\mathbf{G}^{\mathrm{I}}|\mathbf{e}_1^+\rangle$, (b) single slit in a upwardly infinitely thick metal to extract $\mathbf{G}^{\mathrm{II}}|\mathbf{e}_1^-\rangle$, (c) single slit with a finite thickness to extract $\mathbf{G}^{\mathrm{I}}|\mathbf{e}_1^-\rangle$ and $\mathbf{G}^{\mathrm{II}}|\mathbf{e}_1^+\rangle$.

interface II. While the previous explanation assumes a single-mode operation of the aperture, if necessary, we can also extract $\mathbf{G}^{\mathrm{I/II}}|\mathbf{e}_\alpha^\pm\rangle$ of the higher order modes as well for a symmetric aperture, by selectively exciting the desired mode with appropriate boundary conditions at the center plane ($x = 0$ or $y = 0$) of the aperture.

One obvious cost of our method is that we need to have a full dataset of $\mathbf{G}^{\mathrm{I/II}}|\mathbf{e}_\alpha^\pm\rangle$ for the entire xy plane of our interest, which may become computationally expensive to derive directly if the total area of the array exceeds several tens of micrometers in x and y dimensions. We note, however, that the SPP wave generally has the dominant contribution on $\mathbf{G}^{\mathrm{I/II}}|\mathbf{e}_\alpha^\pm\rangle$ over the creeping wave at a distance longer than a few wavelengths from the aperture. Indeed, this will be observed clearly in our example, where $\mathbf{G}^{\mathrm{I}}|\mathbf{e}_1^+\rangle$ quickly converges to the SPP wave (see Fig. 5). Although the creeping wave dominates over the SPP wave again at a very long distance beyond the SPP propagation length [37], [46], [47], it is usually attenuated by a large fraction at such a distance, so that its contribution should have relatively minor contribution to the overall property. As a result, in the regimes sufficiently far from the aperture but not beyond the propagation length of the SPP wave, we can approximate $\mathbf{G}^{\mathrm{I/II}}|\mathbf{e}_\alpha^\pm\rangle$ by a superposition of 2-D SPP waves, which are bounded in the z direction [34]. Such 2-D waves in general are described efficiently by the cylindrical wave decomposition. The x and y components of $\mathbf{G}^{\mathrm{I/II}}|\mathbf{e}_\alpha^\pm\rangle$ in these regions can be thus expressed approximately by $\sum_m c_m H_m^{(1)}(k_{\mathrm{SPP}} r)e^{im\theta}$, where (r, θ) describe the polar coordinate, $H_m^{(1)}$ are the mth-order Hankel functions of the first kind, k_{SPP} is the propagation constant of the SPP, and c_m are the complex amplitudes of these outgoing cylindrical waves. We therefore need to obtain $\mathbf{G}^{\mathrm{I/II}}|\mathbf{e}_\alpha^\pm\rangle$ numerically only in a limited region near the aperture, and then extract the coefficients c_m to describe $\mathbf{G}^{\mathrm{I/II}}|\mathbf{e}_\alpha^\pm\rangle$ over the larger area of our interest. We demonstrate in Section III-A that 20 cylindrical waves are typically sufficient to describe $\mathbf{G}^{\mathrm{I/II}}|\mathbf{e}_\alpha^\pm\rangle$.

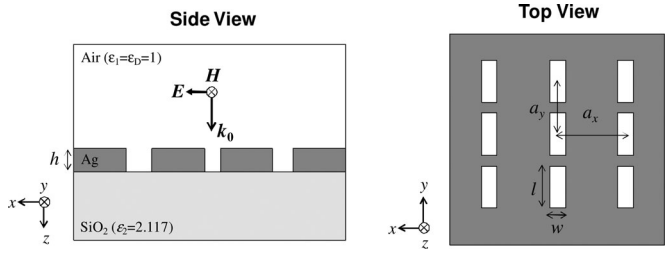

Fig. 3. Structure and the definition of parameters used to study light transmission through a 3×3 array of rectangular slits.

We should note that the final equation (14) is similar to that obtained by Garcia-Vidal *et al.* using the modal expansion technique [22]–[24]. Our scheme, however, is more general in several ways. First, while the modal expansion model uses the plane-wave expansion (Rayleigh expansion) at the top and bottom spaces of the metal film, we do not assume any modal expansion in these regions. Our model is, therefore, applicable to any layered structure, e.g., the top and bottom regions can consist of multiple layers of different dielectric materials. Second, our model does not assume transverse-electric (TE) or transverse-magnetic (TM) modes inside the aperture, so that $|\mathbf{e}_\alpha\rangle$ and $|\mathbf{h}_\alpha\rangle$ can have arbitrary vectorial profiles. Third, we do not employ SIBCs at the metal-dielectric interfaces, an approximation that may cause substantial error especially at a shorter wavelength [26]. Since we extract $\mathbf{G}^{\mathrm{I/II}}|\mathbf{e}_\alpha^\pm\rangle$ numerically, the complicated contributions from both the SPPs and creeping waves are automatically included in the model.

III. Numerical Applications

A. EOT Through a Finite-Sized Slit Array

To verify the validity of the model, we first tested the model in calculating optical transmission through finite-sized periodic arrays of rectangular slits, and compared the results with fully vectorial 3-D-FDTD simulations. Fig. 3 shows the structure considered in this example, where a 3×3 array of rectangular slits ($w = 60$ nm, $l = 300$ nm) is patterned on a silver film ($h = 200$ nm), which lies on top of a silica substrate. We assumed an x-polarized (i.e., electric field pointing in the x direction) plane wave incident normal to the metal surface. The dielectric constant of the metal was modeled by a Lorentz fit to the experimental values [53], where the metallic loss was also included. For simplicity, we ignored the wavelength dispersion of the silica substrate and used $\varepsilon_2 = 2.117$ ($n = 1.455$) for the entire wavelength range of our interest. For the fully vectorial 3-D-FDTD simulation, we used B-CALM, an open-source simulator based on graphical processing units (GPUs) [54].

Fig. 4 shows the propagation constants of the first and the second eigenmodes of a slit with $w = 60$ nm and $l = 300$ nm. Since these two modes converge to the well-known TE_{01} and TE_{02} modes in the perfect conductor limit, we denote them as TE_{01} and TE_{02} throughout this paper. The inset in Fig. 4

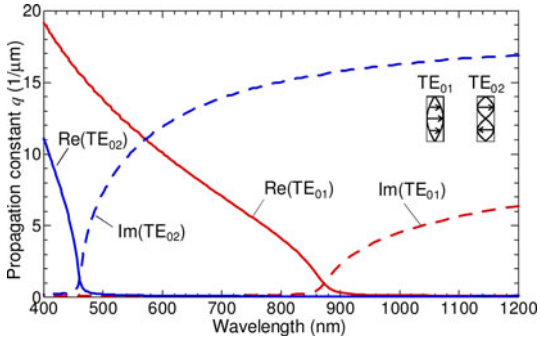

Fig. 4. Real and imaginary parts of the propagation constants for the TE_{01} and TE_{02} modes of a single slit ($w = 60$ nm, $l = 300$ nm) on a silver film. The electric fields inside the slit for the respective modes are illustrated schematically in the inset.

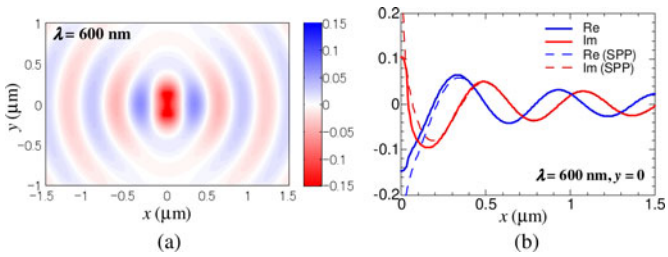

Fig. 5. H_y component of $\mathbf{G}^{\mathrm{I}}|\mathbf{e}^{+}_{\mathrm{TE}_{01}}\rangle$ at 600-nm wavelength: (a) the real part in the xy plane, (b) the real and imaginary parts along the x-axis at $y = 0$ (solid), together with a numerical fit of the SPP mode (dashed), having a dipole radiation pattern in the 2-D plane.

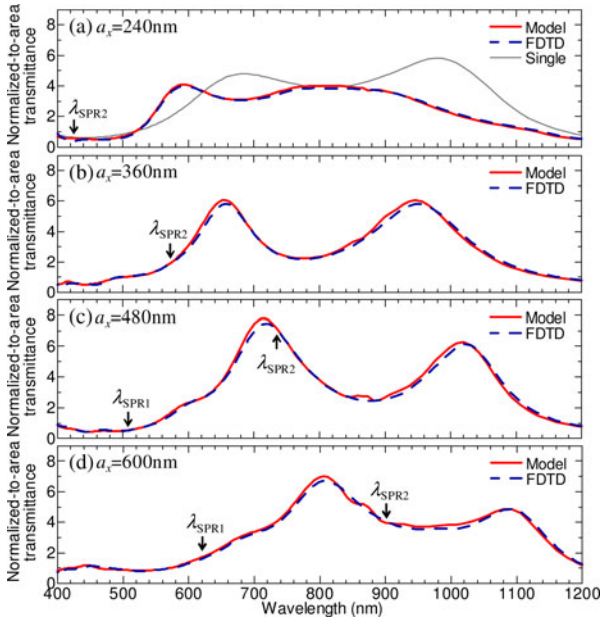

Fig. 6. Normalized-to-area transmittance of a 3×3 slit array (see Fig. 3), calculated by using the model (red solid) and 3-D FDTD (blue dashed) for $a_x = 240, 360, 480$, and 600 nm ($w = 60$ nm, $l = 300$ nm, $h = 200$ nm, $a_y = 360$ nm). Although only the TE_{01} mode is considered in the model, excellent agreement is obtained over a broad spectral range. The arrows indicate the (1,0)-order SPR wavelength at the top (λ_{SPR1}) and bottom (λ_{SPR2}) interfaces. Transmission through a single slit is also plotted in Fig. 6(a) with a gray line.

schematically illustrates the electric field profile inside the slit for these two modes. For this particular geometry, the TE_{01} mode has a cutoff wavelength at 880 nm and becomes evanescent beyond this wavelength. On the other hand, the TE_{02} mode emerges as a propagating mode at a wavelength shorter than 460 nm. Nevertheless, we find that the TE_{02} mode has only minor contribution to the total optical transmission, and thus is neglected in the example case presented in this section. We will, however, show in Section III-B that the TE_{02} mode is essential in calculating the SPP field pattern accurately.

In deriving $\mathbf{G}^{\mathrm{I/II}}|\mathbf{e}^{\pm}_{\alpha}\rangle$, we carried out 3-D-FDTD simulations of the single-slit cases as described in Fig. 2. Exploiting the symmetry of the structure, we used a computational cell that contains only one-quarter of the structure in the $x > 0$ and $y > 0$ region, and applied perfect electrical conductor or perfect magnetic conductor boundary conditions at $x = 0$ and $y = 0$ to selectively excite either the TE_{01} or the TE_{02} mode. Perfect matching layers were used at all the other boundaries. The discretization grid size was set to 5 nm, which showed good convergence in our calculation. Fig. 5 shows the H_y component of $\mathbf{G}^{\mathrm{I}}|\mathbf{e}^{+}_{\mathrm{TE}_{01}}\rangle$ at 600-nm wavelength. In Fig. 5(b), we plot the field along the x-axis at $y = 0$ (solid), together with a numerical fit of the SPP mode (dashed), which is assumed to have a dipole radiation pattern in the 2-D plane [30]. It is clearly observed that the deviation from the SPP mode can be substantial at a short distance. At the same time, $\mathbf{G}^{\mathrm{I}}|\mathbf{e}^{+}_{\mathrm{TE}_{01}}\rangle$ converges to the SPP mode after a distance longer than a half the wavelength, which supports the validity of approximating $\mathbf{G}^{\mathrm{I}}|\mathbf{e}^{+}_{\mathrm{TE}_{01}}\rangle$ by cylindrical waves at these regimes as discussed in Section II-B.

Using the dataset of $q_\alpha, |\mathbf{e}_{t\alpha}\rangle, \mathbf{G}^{\mathrm{I/II}}|\mathbf{e}^{\pm}_{\alpha}\rangle$, and $|\mathbf{H}^{\mathrm{I}}_{0}\rangle$stored in advance, $\{C_\alpha, D_\alpha\}$ in (14) were solved for a given location of slits, from which the total transmission was calculated. For this example of nine slits, the computation took less than 2 s per wavelength on a 2.13-GHz Quad Core processor. This is a dramatic speed up compared with full-field 3-D-FDTD simulation of the entire structure, which took more than 90 min on an NVIDIA C-1060 GPU [54]. Out of the 2-s total computation time in our model, roughly 1 s was used for loading $|\mathbf{e}_{t\alpha}\rangle$ and $\mathbf{G}^{\mathrm{I/II}}|\mathbf{e}^{\pm}_{\alpha}\rangle$, and most of the remaining time was used for computing $\langle\mathbf{e}_{t\alpha}|\,\mathbf{G}^{\mathrm{I/II}}|\mathbf{e}^{\pm}_{\beta}\rangle$ to populate the matrix. Depending on the application, therefore, we could achieve further speed up by computing $\langle\mathbf{e}_{t\alpha}|\,\mathbf{G}^{\mathrm{I/II}}|\mathbf{e}^{\pm}_{\beta}\rangle$ as a function of the slit separation in advance.

Fig. 6 shows the comparison of transmission spectra calculated using the model (red solid) and the fully vectorial 3-D-FDTD simulation of entire structure (blue dashed). The results are plotted for different values of a_x (240, 360, 480, and 600 nm) with $a_y = 360$ nm. For these cases, the minimal separation between the apertures is 60 nm and is sufficiently larger than the skin depth of the silver, which is less than 15 nm in the wavelength range of our interest (400–1200 nm). The transmission was evaluated at the middle of the metal film and normalized to the total area of the nine slits, following the usual convention [24]. A transmission over 1, therefore, corresponds to EOT. Although we have only considered the TE_{01} mode in the model,

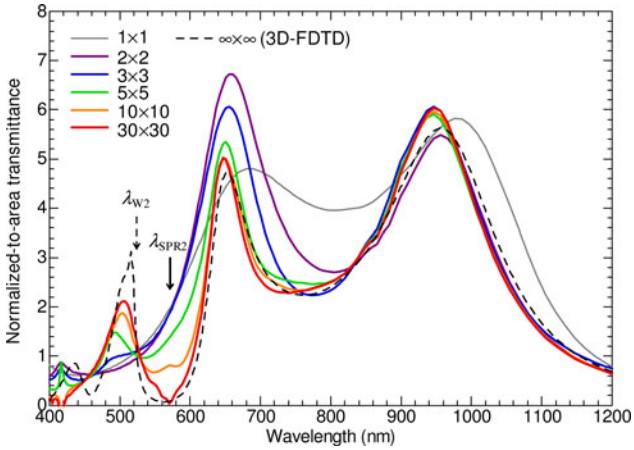

Fig. 7. Normalized-to-area transmittance through an $N \times N$ array for increasing N ($w = 60$ nm, $l = 300$ nm, $h = 200$ nm, $a_x = a_y = 360$ nm). For $N > 3$, the cylindrical wave expansion is employed to approximately calculate $\kappa_{\alpha\beta}^{ij}$ between widely separated slits. As N increases, the transmission spectrum converges to that of an infinite array (black dashed line), which is obtained by 3-D FDTD simulation with periodic boundary walls. The first-order SPR wavelength $\lambda_{\mathrm{SPR}2}$ and the Rayleigh–Wood anomaly λ_{W2} at the bottom interface are indicated by the solid and dashed arrows, respectively.

excellent agreement is obtained in all cases over a broad spectral range (400–1200 nm).

We should note that the resonant excitation of SPPs at the top and bottom metal interfaces, which has been considered as the dominant mechanism responsible for EOT in deeply subwavelength nanohole arrays [26], [55]–[57], plays rather an indirect role in Fig. 6 due to the presence of propagating modes inside the slits [58]. To illustrate this point, the lowest (1,0)-order surface-plasmon-resonance (SPR) wavelengths at the two interfaces, defined by $\lambda_{\mathrm{SPR}} \equiv a_x \sqrt{\mathrm{Re}\left[\varepsilon_{\mathrm{M}} \varepsilon_j / (\varepsilon_{\mathrm{M}} + \varepsilon_j)\right]}$ ($j = 1$, 2) [26], [58], are indicated by arrows in Fig. 6, which, indeed, do not correspond directly to the spectral peaks. On the other hand, the normalized-to-area transmission through a single slit is plotted in Fig. 6(a) with a gray solid line, which, even in the absence of multiple-slit SPRs, already exhibits clear EOT peaks. From the dispersion curve [see Fig. 5(a)] and the field inside the slit (not shown), it is confirmed that the two spectral peaks around 980 and 680 nm correspond, respectively, to the first- and second-order Fabry–Perot resonances of the TE_{01} mode inside the slit. In the presence of other slits, the effective reflection coefficients of the TE_{01} mode at the top and bottom interfaces should be modified [59], [60], which results in the spectral shift of these two Fabry–Perot resonances as evidenced in Fig. 6(a)–(d).

It is of further interest to evaluate how the transmission spectrum converges to that of an infinite array as we increase the number of slits [24], [26]. As discussed in Section II-B, we can approximately calculate $\mathbf{G}^{\mathrm{I/II}} |\mathbf{e}_\alpha^{\pm}\rangle$ in a broader area by using the cylindrical wave decomposition. Fig. 7 shows the transmission spectrum calculated by using the model with an increasing number of slits for $a_x = a_y = 360$ nm. We employed 20 modes for the cylindrical wave decomposition. We also plot in Fig. 7 the exact solution for an infinite array, calculated by 3-D-FDTD with the use of periodic boundary conditions. We see that the transmission spectrum converges to that of the infinite array with an increasing number of slits, which justifies the validity of our approximate method using the cylindrical wave decomposition. More specifically, as the number of slits increases, the transmission spectrum transforms into a Fano-type asymmetric lineshape [30], [61], [62]. A transmission dip emerges at 572 nm, which corresponds exactly to the (1,0)-order SPR wavelength at the bottom silver-silica interface ($\lambda_{\mathrm{SPR}2}$) as defined previously. In addition, a sharp peak develops near the corresponding Rayleigh–Wood anomaly, defined by $\lambda_{\mathrm{W}j} \equiv a_x \sqrt{\varepsilon_j}$ $= 523.8$ nm [30]. The fact that the SPR can actually suppress the transmission and the transmission peaks can instead correspond with the appearance of Rayleigh–Wood anomalies has been observed in infinite 1-D and 2-D slit arrays [58]–[64], [27], [28]. Our model not only reproduces these previous findings, but also reveals explicitly the effects of finite array size, including how these dips and peaks emerge and develop with an increasing number of apertures.

More interestingly, we also find from Fig. 7 that the normalized-to-area transmission at around 660 nm is maximized for the 2×2 array and decreases for larger sized arrays. Such a feature is in contrast to the previous findings on circular nanohole arrays, where the EOT is enhanced monotonically with increasing number of holes [24], [26]. Aside from a theoretical interest in such counterintuitive behavior, the existence of an optimal array size has substantial implications for practical applications. For a given incident beam condition, an optimized design of a finite-sized array should exist to maximize the total transmission. The present method should particularly be useful in deriving such an optimized design with less computational effort.

B. Surface Plasmon Excitation by Arbitrary Array of Slits

One of the strengths of the present method is that it should be applicable to a completely arbitrary pattern of apertures as long as they are separated by a distance that is sufficiently large compared to the skin depth of the metal. To verify this feature, we study excitation of SPP waves by 10 arbitrarily located slits on a silver film as illustrated in the inset of Fig. 8. The dimensional parameters of each slit are the same as those in the previous section; $w = 60$ nm, $l = 300$ nm, and $h = 200$ nm. Because here we want to examine the detailed field distribution, we need to include the effects of asymmetric excitation of eigenmodes inside the slits; as a result, we find that in addition to the fundamental TE_{01} mode, the TE_{02} mode must also be included in deriving the SPP field pattern accurately.

Fig. 8 shows the amplitudes A_α (B_α) of the forward (backward)-propagating TE_{01} and TE_{02} modes inside the ten slits at 600-nm wavelength, derived using the model. The results obtained by 3-D FDTD of the entire structure are also plotted with crosses, which agree excellently with the model. From $\{A_\alpha, B_\alpha\}$ and $\mathbf{G}^{\mathrm{I/II}} |\mathbf{e}_\alpha^{\pm}\rangle$, we can then calculate the excited SPP field at arbitrary locations. Fig. 9 shows the field distribution of the E_z component (600-nm wavelength) at the bottom silver-silica interface, obtained using the model [see Fig. 9(a)] and 3-D-FDTD [see Fig. 9(b)]. We see that the local resonances

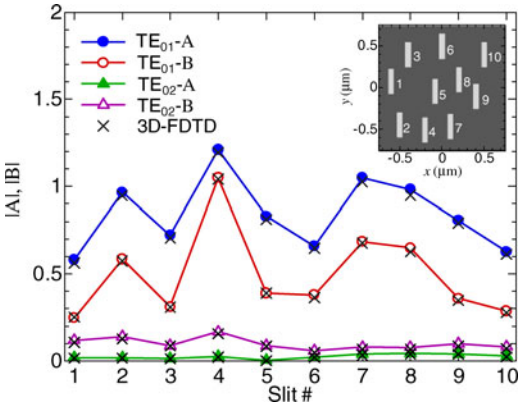

Fig. 8. Absolute values of A (forward-propagating amplitude) and B (backward-propagating amplitude) of TE_{01} and TE_{02} modes inside the ten slits (inset) at 600-nm wavelength, calculated using the model. The slit parameters and the cross-sectional structure are the same as in Fig. 3 ($w = 60$ nm, $l = 300$ nm, $h = 200$ nm). Good agreement is obtained with the 3-D FDTD simulations (crosses). The lines between the markers are guides for the eye.

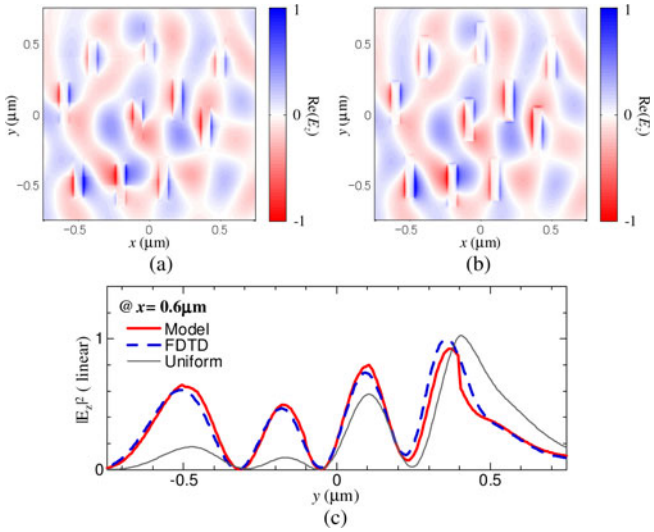

Fig. 9. E_z field at the bottom silver-silica interface at 600-nm wavelength calculated using (a) the model and (b) 3-D FDTD. (c) E_z field intensity at $x = 0.6$ μm. The field calculated using uniform excitation approximation is also shown by a gray solid line.

(e.g., at slits #2 and #4) are captured accurately and the field distribution is reproduced well by using the model. Fig. 9(c) quantitatively compares the E_z field intensity at $x = 0.6$ μm. For comparison, we also plot the field obtained by assuming that all 10 slits are excited uniformly with the excitation efficiency calculated for a single aperture (gray solid line). While the simple uniform excitation approximation fails in reproducing the SPP field, quantitative agreement is obtained by our model. These results clearly reveal the importance of modeling the multislit interactions accurately, which does significantly influence the overall optical properties.

IV. Conclusion

We have demonstrated a powerful method of analyzing the optical properties of a 3-D metal film with an arbitrarily patterned finite-sized array of subwavelength apertures. The model treats each aperture as a *modal source radiator* and uses its radiation patterns to analyze the coupling between different radiators. Owing to the limited number of relevant eigenmodes inside the subwavelength apertures, the problem is efficiently cast into a small-rank linear system of equations. We have also presented a straightforward method to derive all the necessary radiation patterns through numerical simulations of single-aperture cases. The fields at larger areas could also be obtained by the use of cylindrical wave decomposition. We have verified the method in few test cases by comparing with the fully vectorial 3-D-FDTD solutions. The method has accurately reproduced EOT spectra and Fano resonances in 2-D nanoslit arrays, as well as the complex SPP field pattern excited by an aperiodic nanoslit array. We have also explored the dependence of EOT on array size and discovered a novel regime, where the EOT efficiency decreases with an increasing number of nanoslits.

Although we have treated arrays of identical rectangular nanoslits as example cases in this paper, the method should in principle be applicable to subwavelength apertures of arbitrary geometries, provided that the field inside the apertures can be approximated by the fundamental eigenmode or a few eigenmodes with symmetrical constraints. In addition, the method should also be effective for any multilayered structure; e.g., the top and bottom regions can consist of multiple layers of different dielectric materials. The dramatic reduction of computation time, together with the straightforward implementation using any commercial full-field simulator, makes the present method highly attractive for practical applications. The method could, for example, be employed in iterative design of a variety of novel aperiodic plasmonic devices [18]–[21].

Acknowledgment

T. Tanemura would like to thank K. C. Balram, V. Liu, Z. Ruan, P. B. Catrysse, and L. Verslegers for valuable discussions during this work.

References

[1] T. W. Ebbesen, H. J. Lezec, H. F. Ghaemi, T. Thio, and P. A. Wolff, "Extraordinary optical transmission through sub-wavelength hole arrays," *Nature*, vol. 391, pp. 667–669, 1998.

[2] H. J. Lezec, A. Degiron1, E. Devaux1, R. A. Linke, L. Martin-Moreno, F. J. Garcia-Vidal, and T. W. Ebbesen, "Beaming light from a subwavelength aperture," *Science*, vol. 297, pp. 820–822, 2002.

[3] S. Zhang, W. Fan, N. C. Panoiu, K. J. Malloy, R. M. Osgood, and S. R. J. Brueck, "Experimental demonstration of near-infrared negative-index metamaterials," *Phys. Rev. Lett.*, vol. 95, pp. 137404-1–137404-4, 2005.

[4] S. M. Williams, K. R. Rodriguez, S. Teeters-Kennedy, A. D. Stafford, S. R. Bishop, U. K. Lincoln, and J. V. Coe, "Use of the extraordinary infrared transmission of metallic subwavelength arrays to study the catalyzed reaction of methanol to formaldehyde on copper oxide," *J. Phys. Chem. B*, vol. 108, pp. 11833–11837, 2004.

[5] J. Eid, A. Fehr, J. Gray, K. Luong, J. Lyle, G. Otto, P. Peluso, D. Rank, P. Baybayan, B. Bettman, A. Bibillo, K. Bjornson, B. Chaudhuri, F. Christians, R. Cicero, S. Clark, R. Dalal, A. de Winter, J. Dixon, M. Foquet, A. Gaertner, P. Hardenbol, C. Heiner, K. Hester, D. Holden, G. Kearns, X. Kong, R. Kuse, Y. Lacroix, S. Lin, P. Lundquist, C. Ma, P. Marks, M. Maxham, D. Murphy, I. Park, T. Pham, M. Phillips, J. Roy, R. Sebra, G. Shen, J. Sorenson, A. Tomaney, K. Travers, M. Trulson, J. Vieceli, J. Wegener, D. Wu, A. Yang, D. Zaccarin, P. Zhao, F. Zhong, J. Korlach, and S. Turner, "Real-time DNA sequencing from single Polymerase molecules," *Science*, vol. 323, pp. 133–138, 2009.

[6] R. Gordon, A. G. Brolo, D. Sinton, and K. L. Kavanagh, "Resonant optical transmission through hole-arrays in metal films: physics and applications," *Laser Photon. Rev.*, vol. 4, pp. 311–335, 2010.

[7] C. Liu, V. Kamaev, and Z. V. Vardeny, "Efficiency enhancement of an organic light-emitting diode with a cathode forming two-dimensional periodic hole array," *Appl. Phys. Lett.*, vol. 86, pp. 143501-1–143501-3, 2005.

[8] Y. Gong, J. Lu, S. L. Cheng, Y. Nishi, and J. Vuckovic, "Plasmonic enhancement of emission from Si-nanocrystals," *Appl. Phys. Lett.*, vol. 94, pp. 013106-1–013106-3, 2009.

[9] T. Ishi, J. Fujikata, K. Makita, T. Baba, and K. Ohashi, "Si nano-photodiode with a surface plasmon antenna," *Jpn. J. Appl. Phys.*, vol. 44, pp. L364–L366, 2005.

[10] L. Tang, D. A. B. Miller, A. K. Okyay, J. A. Matteo, Y. Yuen, K. C. Saraswat, and L. Hesselink, "C-shaped nanoaperture-enhanced germanium photodetector," *Opt. Lett.*, vol. 31, pp. 1519–1521, 2006.

[11] L. Tang, S. Latif, and D. A. B. Miller, "Plasmonic device in silicon CMOS," *Electron. Lett.*, vol. 45, pp. 706–708, 2009.

[12] R. A. Pala, J. White, E. Barnard, J. Liu, and M. L. Brongersma, "Design of plasmonic thin-film solar cells with broadband absorption enhancements," *Adv. Mater.*, vol. 21, pp. 3504–3509, 2009.

[13] C. Min, J. Li, G. Veronis, J.-Y. Lee, S. Fan, and P. Peumans, "Enhancement of optical absorption in thin-film organic photovoltaic solar cells through the excitation of plasmonic modes in metallic gratings," *Appl. Phys. Lett.*, vol. 96, pp. 133302-1–133302-3, 2010.

[14] Z. Ruan and M. Qiu, "Enhanced transmission through periodic arrays of subwavelength holes: the role of localized waveguide resonances," *Phys. Rev. Lett.*, vol. 96, pp. 233901-1–233901-4, 2006.

[15] M. Sun, J. Tian, S. Han, Z. Li, B. Cheng, D. Zhang, A. Jin, and H. Yang, "Effect of the subwavelength hole symmetry on the enhanced optical transmission through metallic films," *J. Appl. Phys.*, vol. 100, pp. 024320-1–024320-4, 2006.

[16] F. Przybilla, C. Genet, and T. W. Ebbesen, "Enhanced transmission through Penrose subwavelength hole arrays," *Appl. Phys. Lett.*, vol. 89, pp. 121115-1–121115-3, 2006.

[17] T. Matsui, A. Agrawal, A. Nahata, and Z. V. Vardeny, "Transmission resonances through aperiodic arrays of subwavelength apertures," *Nature*, vol. 446, pp. 517–521, 2007.

[18] L. Verslegers, P. B. Catrysse, Z. Yu, J. S. White, E. S. Barnard, M. L. Brongersma, and S. Fan, "Planar lenses based on nanoscale slit arrays in a metallic film," *Nano Lett.*, vol. 9, pp. 235–238, 2009.

[19] L. Lin, X. M. Goh, L. P. McGuinness, and A. Roberts, "Plasmonic lenses formed by two-dimensional nanometric cross-shaped aperture arrays for Fresnel-region focusing," *Nano Lett.*, vol. 10, pp. 1936–1940, 2010.

[20] L. Verslegers, P. B. Catrysse, Z. Yu, and S. Fan, "Planar metallic nanoscale slit lenses for angle compensation," *Appl. Phys. Lett.*, vol. 95, pp. 071112-1–071112-3, 2009.

[21] T. Tanemura, K. C. Balram, D. S. Ly-Gagnon, P. Wahl, J. S. White, M. L. Brongersma, and D. A. B. Miller, "Multiple-wavelength focusing of surface plasmons with a nonperiodic nanoslit coupler," *Nano Lett.*, vol. 11, pp. 2693–2698, 2011.

[22] J. Bravo-Abad, L. Martin-Moreno, and F. J. Garcia-Vidal, "Resonant transmission of light through subwavelength holes in thick metal films," *IEEE J. Sel. Top. Quantum Electron.*, vol. 12, no. 6, pp. 1221–1227, Nov./Dec. 2006.

[23] J. Bravo-Abad, A. I. Fernandez-Dominguez, F. J. Garcia-Vidal, and L. Martin-Moreno, "Theory of extraordinary transmission of light through quasiperiodic arrays of subwavelength holes," *Phys. Rev. Lett.*, vol. 99, pp. 203905-1–203905-4, 2007.

[24] F. J. Garcia-Vidal, L. Martin-Moreno, T. W. Ebbesen, and L. Kuipers, "Light passing through subwavelength apertures," *Rev. Mod. Phys.*, vol. 82, pp. 729–787, 2010.

[25] F. J. Garcia-Vidal, L. Martin-Moreno, E. Moreno, L. K. S. Kumar, and R. Gordon, "Transmission of light through a single rectangular hole in a real metal," *Phys. Rev. B*, vol. 74, pp. 153411-1–153411-4, 2006.

[26] F. Przybilla, A. Degiron, C. Genet, T.W. Ebbesen, F. de Leon-Perez, J. Bravo-Abad, F. J. Garcia-Vidal, and L. Martin-Moreno, "Efficiency and finite size effects in enhanced transmission through subwavelength apertures," *Opt. Exp.*, vol. 16, pp. 9571–9579, 2008.

[27] H. Liu and P. Lalanne, "Microscopic theory of the extraordinary optical transmission," *Nature*, vol. 452, pp. 728–731, 2008.

[28] H. Liu and P. Lalanne, "Comprehensive microscopic model of the extraordinary optical transmission," *J. Opt. Soc. Am. A*, vol. 27, pp. 2542–2550, 2010.

[29] X. Huang and M. L. Brongersma, "Rapid computation of light scattering from aperiodic plasmonic structures," *Phys. Rev. B*, vol. 84, pp. 245120-1–245120-7, 2011.

[30] S. H. Chang, S. K. Gray, and G. C. Schatz, "Surface plasmon generation and light transmission by isolated nanoholes and arrays of nanoholes in thin metal films," *Opt. Exp.*, vol. 13, pp. 3150–3165, 2005.

[31] E. Popov, M. Neviere, S. Enoch, and R. Reinisch, "Theory of light transmission through subwavelength periodic hole arrays," *Phys. Rev. B*, vol. 62, pp. 16100–16108, 2000.

[32] M. Paulus and O. J. F. Martin, "Light propagation and scattering in stratified media: A Green's tensor approach," *J. Opt. Soc. Am. A*, vol. 18, pp. 854–861, 2001.

[33] Y. Alaverdyan, B. Sepulveda, L. Eurenius, E. Olsson, and M. Käll, "Optical antennas based on coupled nanoholes in thin metal films," *Nature Phys.*, vol. 3, pp. 884–889, 2007.

[34] J. Alegret, P. Johansson, and M. Käll, "Green's tensor calculations of plasmon resonances of single holes and hole pairs in thin gold films," *New J. Phys.*, vol. 10, pp. 105004-1–105004-13, 2008.

[35] J. Alegret, M. Käll, and P. Johansson, "Top-down extended meshing algorithm and its applications to Green's tensor nano-optics calculations," *Phys. Rev. E*, vol. 75, pp. 046702-1–046702-8, 2007.

[36] N. B. Piller and O. J. F. Martin, "Increasing the performance of the coupled-dipole approximation: A spectral approach," *IEEE Trans. Antenna Propag.*, vol. 46, no. 8, pp. 1126–1137, Aug. 1998.

[37] P. Johansson, "Electromagnetic Green's function for layered systems: Applications to nanohole interactions in thin metal films," *Phys. Rev. B*, vol. 83, pp. 195408-1–195408-14, 2011.

[38] M. Paulus, P. Gay-Balmaz, and O. J. F. Martin, "Accurate and efficient computation of the Green's tensor for stratified media," *Phys. Rev. E*, vol. 62, pp. 5797–5807, 2000.

[39] E. Simsek, Q. H. Liu, and B. Wei, "Singularity subtraction for evaluation of Green's functions for multilayer media," *IEEE Trans. Microw. Theory Tech.*, vol. 54, no. 1, pp. 216–225, Jan. 2006.

[40] G. Gay, O. Alloschery, B. Viaris De Lesegno, C. O'Dwyer1, J. Weiner, and H. J. Lezec, "The optical response of nanostructured surfaces and the composite diffracted evanescent wave model," *Nature Phys.*, vol. 2, pp. 262–267, 2006.

[41] P. Lalanne and J. P. Hugonin, "Interaction between optical nano-objects at metallo-dielectric interfaces," *Nature Phys.*, vol. 2, pp. 551–556, 2006.

[42] L. Chen, J. T. Robinson, and M. Lipson, "Role of radiation and surface plasmon polaritons in the optical interactions between a nano-slit and a nano-groove on a metal surface," *Opt. Exp.*, vol. 14, pp. 12629–12636, 2006.

[43] L. Aigouy, P. Lalanne, J. P. Hugonin, G. Julie, V. Mathet, and M. Mortier, "Near-field analysis of surface waves launched at nanoslit apertures," *Phys. Rev. Lett.*, vol. 98, pp. 153902-1–153902-4, 2007.

[44] X. Y. Yang, H. T. Liu, and P. Lalanne, "Cross conversion between surface plasmon polariton and quasicylindrical waves," *Phys. Rev. Lett.*, vol. 102, pp. 153903-1–153903-4, 2009.

[45] W. Dai and C. M. Soukoulis, "Theoretical analysis of the surface wave along a metal-dielectric interface," *Phys. Rev. B*, vol. 80, pp. 155407-1–155407-4, 2009.

[46] A. Y. Nikitin, S. G. Rodrigo, F. J. Garcia-Vidal, and L. Martin-Moreno, "In the diffraction shadow: Norton waves versus surface plasmon polaritions in the optical region," *New J. Phys.*, vol. 11, pp. 123020-1–123020-15, 2009.

[47] A. Y. Nikitin, F. J. Garcia-Vidal, and L. Martin-Moreno, "Surface electromagnetic field radiated by a subwavelength hole in a metal film," *Phys. Rev. Lett.*, vol. 105, pp. 073902-1–073902-4, 2010.

[48] F. V. Beijnum, C. Retif, C. B. Smiet, and M. P. van Exter, "Transmission processes in random patterns of subwavelength holes," *Opt. Lett.*, vol. 36, pp. 3666–3668, 2011.

[49] E. M. Purcell and C. R. Pennypacker, "Scattering and absorption of light by nonspherical dielectric grains," *Astrophys. J.*, vol. 186, pp. 705–714, 1973.

[50] B. T. Draine and P. J. Flatau, "Discrete-dipole approximation for scattering calculations," *J. Opt. Soc. Am. A*, vol. 11, pp. 1491–1499, 1994.

[51] A. W. Snyder and J. D. Love, *Optical Waveguide Theory*. London, U.K.: Chapman and Hall, 1983.

[52] S. E. Kocabas, G. Veronis, D. A. B. Miller, and S. Fan, "Modal analysis and coupling in metal-insulator-metal waveguides," *Phys. Rev. B*, vol. 79, pp. 035120-1–035120-17, 2009.

[53] E. D. Palik, *Handbook of Optical Constants of Solids*. New York: Academic, 1985.

[54] P. Wahl, D. S. Ly-Gagnon, C. Debaes, D. A.B. Miller, and H. Thienpont, "B-CALM: An open-source GPU-based 3D-FDTD with multi-pole dispersion for plasmonics," *Opt. Quantum Electron.*, vol. 44, pp. 285–290, 2012.

[55] J. A. Porto, F. J. Garcia-Vidal, and J. B. Pendry, "Transmission resonances on metallic gratings with very narrow slits," *Phys. Rev. Lett.*, vol. 83, pp. 2945–2848, 1999.
[56] L. Martin-Moreno, F. J. Garcia-Vidal, H. J. Lezec, K. M. Pellerin, T. Thio, J. B. Pendry, and T. W. Ebbesen, "Theory of extraordinary optical transmission through subwavelength hole arrays," *Phys. Rev. Lett.*, vol. 86, pp. 1114–1117, 2001.
[57] W. L. Barnes, W. A. Murray, J. Dintinger, E. Devaux, and T. W. Ebbesen, "Surface plasmon polaritons and their role in the enhanced transmission of light through periodic arrays of subwavelength holes in a metal film," *Phys. Rev. Lett.*, vol. 92, pp. 107401-1–107401-4, 2004.
[58] P. B. Catrysse and S. Fan, "Propagating plasmonic mode in nanoscale apertures and its implications for extraordinary transmission," *J. Nanophotonics*, vol. 2, pp. 021790-1–021790-20, 2008.
[59] Y. Ding, J. Yoon, M. H. Javed, S. H. Song, and R. Magnusson, "Mapping surface-plasmon polaritons and cavity modes in extraordinary optical transmission," *IEEE Photon. J.*, vol. 3, no. 3, pp. 365–374, Jun. 2011.
[60] Q. Cao and P. Lalanne, "Negative role of surface plasmons in the transmission of metallic gratings with very narrow slits," *Phys. Rev. Lett.*, vol. 88, pp. 057403-1–057403-4, 2002.
[61] C. Genet, M. P. van Exter, and J. P. Woerdman, "Fano-type interpretation of red shifts and red tails in hole array transmission spectra," *Opt. Commun.*, vol. 225, pp. 331–336, 2003.
[62] M. Sarrazin, J. P. Vigneron, and J. M. Vigoureux, "Role of Wood anomalies in optical properties of thin metallic films with a bidimensional array of subwavelength holes," *Phys. Rev. B*, vol. 67, pp. 085415-1–085415-8, 2003.
[63] Y. Xie, A. R. Zakharian, J. V. Moloney, and M. Mansuripur, "Transmission of light through a periodic array of slits in a thick metallic film," *Opt. Exp.*, vol. 13, pp. 4485–4491, 2005.
[64] C. Huang, Q. Wang, and Y. Zhu, "Dual effect of surface plasmons in light transmission through perforated metal films," *Phys. Rev. B*, vol. 75, pp. 245421-1–245421-7, 2007.

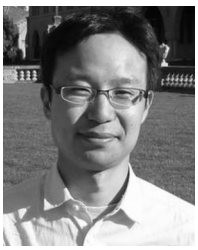

Takuo Tanemura (S'02–M'06) received the B.E., M.S., and Ph.D. degrees in electronic engineering, all from The University of Tokyo, Tokyo, Japan, in 2001, 2003, and 2006, respectively.

In 2006, he joined the Department of Electrical Engineering, The University of Tokyo, where he moved to the Research Center for Advanced Science and Technology in 2007 as a Lecturer. In April 2012, he moved back to the Department of Electrical Engineering, The University of Tokyo, and became an Associate Professor. From March 2010 to February 2012, he was a Visiting Scholar at Ginzton Laboratory, Stanford University. His research interest includes semiconductor photonic integrated circuits, nanophotonic and nanometallic devices, photonic switching networks, and optical interconnects.

Dr. Tanemura is a member of the Institute of Electronics, Information and Communication Engineers of Japan. He received the 2005 IEEE Photonics Society Graduate Student Fellowships and Ericsson Young Scientist Award 2006.

Pierre Wahl received the B.S. degree in electrical engineering and the Erasmus Mundus M.S. degree in photonics from Vrije Universiteit Brussel, Brussels, Belgium, in 2007 and 2010, respectively, where he is currently working toward the Ph.D. degree in electrical engineering at the Brussels Photonics Group on low energy optical interconnects. His Master's thesis at the Interuniversity Microelectronics Center, Leuven, Belgium, in 2010, was on high-frequency electrical voltage-controlled oscillators.

He joined the Miller Group, Stanford University, Stanford, CA, as a Visiting Researcher from 2010 to July 2011. His current research interests include optical interconnects and advanced simulation and optimization methods in nanophotonics.

Mr. Wahl has been a member of the International Society for Optics and Photonics since 2010.

Shanhui Fan (F'11) received the Ph.D. degree in theoretical condensed matter physics from the Massachusetts Institute of Technology (MIT), Cambridge, in 1997.

He is currently a Professor of electrical engineering at Stanford University, Stanford, CA. He was a Research Scientist at the Research Laboratory of Electronics, MIT. He has published more than 250 refereed journal articles that were cited over 15 000 times, has given more than 180 invited talks, and was granted 43 U.S. patents. His research interests include computational and theoretical studies of solid state and photonic structures and devices, especially photonic crystals, plasmonics, and metamaterials.

Dr. Fan received the National Science Foundation Career Award in 2002, the David and Lucile Packard Fellowship in Science and Engineering in 2003, the National Academy of Sciences Award for Initiative in Research in 2007, and the Adolph Lomb Medal from the Optical Society of America in 2007. He is a Fellow of the American Physical Society, the Optical Society of America, and the SPIE.

David A. B. Miller (F'95) received the Ph.D. degree in physics from Heriot-Watt University, Edinburgh, U.K., in 1979.

He was with Bell Laboratories from 1981 to 1996, where he was a Department Head from 1987. He is currently the W. M. Keck Professor of electrical engineering, and a Co-Director of the Stanford Photonics Research Center at Stanford University, Stanford, CA. He has published more than 250 scientific papers and the text *Quantum Mechanics for Scientists and Engineers*, and holds 69 patents. His research interests include physics and devices in nanophotonics, nanometallics, and quantum-well optoelectronics, and fundamentals and applications of optics in information sensing, switching, and processing.

Dr. Miller is a Fellow of the Optical Society of America, American Physical Society, the Royal Society of London, and the Royal Society of Edinburgh, holds two honorary degrees, and is a member of the U.S. National Academy of Sciences and the U.S. National Academy of Engineering. He has been active in professional societies and was the President of the IEEE Lasers and Electro-Optics Society in 1995. He has also received numerous awards.